DEEP LEARNING APPROACH
FOR THE IDENTIFICATION OF STRUCTURAL LAYERS
IN HISTORIC MONUMENTS FROM GROUND
PENETRATING RADAR IMAGES

Alexakis E.[1], Lampropoulos K.[1], Doulamis N.[2], Doulamis A.[2], Moropoulou A.[1]

*[1]Laboratory of Materials Science and Engineering, School of Chemical Engineering,
National Technical University of Athens, Athens, Greece*
[2]School of Rural and Surveying Engineering, National Technical University of Athens, Athens, Greece

ABSTRACT

The present work is about the application of Artificial Intelligence and in particular Computer Vision approaches for the analysis and classification of Ground Penetrating Radar (GPR) B-Scan radargrams gathered during a GPR data acquisition campaign for the diagnostic study, for the assessment of the preservation state of the Holy Aedicule of the Holy Sepulchre in Jerusalem. The analysis of those data revealed the Aedicule's structural layers and most important indicated the cause of the historical building pathology. The objective of this study is to extract the knowledge coming from the typical analysis of B-Scan radargrams, based on which the various structural layers derived, omitting this way several manual data pre-processing and time-consuming steps. The study employs a Deep Learning architecture, known as U-Net, where an image segmentation approach has been followed to build and train a classifier able to discriminate the various structural layers detected by the original measurements of radargrams.

1. INTRODUCTION

Non-Destructive Testing (NDT) comprise of a wide group of techniques finding use in the science, technology, and industry sectors mainly for the evaluation of the material/component/system properties by causing the minimum possible damage (Cartz, 1995). When it comes to cultural heritage assets (e.g., monuments), one of the most prominent aspects to be considered for the assessment of the preservation state, is its integrity affection to the minimum possible extend throughout the diagnostic process. Thus, NDT approaches are widely utilized for minimal invasion as they could provide important knowledge regarding the current preservation state of the monument (Anzani et al., 2006; Martini et al., 2017; Moropoulou et al., 2018). Even though that such techniques play an important role to the historic building diagnostics and monitoring, each one of them presents certain limitations that could be overcome even by combining with various NDTs or/and with Artificial Intelligence (AI) and Machine Learning (ML) approaches. On the one hand, combining various Non-Destructive Techniques (NDTs) has been already managed for diagnostic, maintenance, and monitoring purposes for various case studies (Alexakis et al., 2018; Vidovszky, 2016), suggesting the NDTs as an ideal tool to determine pathology before any interventions and monitor the effects after it will take place. On the other hand, the emergence of AI has provided researchers with new innovative tools to enhance traditional approaches (Fiorucci et al., 2020; Garrido et al., 2021).

Ground Penetrating Radar (GPR) technique, seem to gather great interest as an NDT approach considering the various applications from implementing archaeo-geophysical methods of prospection over buried ancient structures (Savvaidis et al, 1999; Levy et al., 2018; Jaén-Candón et al., 2019) to object/target detection and identification of structural patterns in monuments (Lampropoulos et al., 2017; Aydıngün et al., 2020) where complex computational techniques are applied highlighting the GPR's importance throughout the diagnosis process over complex historical structures that is practically demonstrated in cases such as: revealing structural layers, defect areas and voids etc. This is due to GPR's advantages such as portability, low cost and reasonable budget of the initial investment, ease of data acquisition, high versatility in terms of multipurpose applications, as it can be utilized from infrastructure maintenance and large area surveys to environmental investigations and cultural heritage protection.

On top of those, the ascent of AI and ML have brought evolution in the NDTs and subsequently the GPR research sector. For example, GPR data enhancement by generating high-precision GPR images utilizing Least Square Generative Adversarial Networks (Yue et al., 2021). Moreover, regarding the GPR data interpretation process for semi-automatic feature extraction (Leckebusch, J. et al., 2008), underground object classification with the use of GPR 3D data. Last but not least, an interesting study is about the automatic feature extraction from archaeo-geophysical GPR B-Scans, utilizing deep learning approaches and particularly a U-Net Neural Network (NN) architecture way similar to the one used in the present study (Küçükdemirci and Sarris, 2019). The outcome of this study regarding the prediction of the patterns (anomalies) and the background, is quite satisfying, but still the amount of annotated/labeled data needed to efficiently train the model is not enough.

Despite the advances, the most prominent disadvantage of GPR is the need of data post processing not only during their acquisition but also later at the interpretation and assessment phase (Travassos et al., 2020) whereas utilizing AI and ML approaches for data interpretation is quite challenging due to the great amount of data needed to train and validate a well performing Artificial Neural Network (Manataki et al., 2021). Signal processing is a prerequisite step to filter out irrelevant and keep useful information and is not advisable to be automated as different use cases might have different needs (i.e., increased resolution instead of high penetration depth) whereas pattern recognition automation could enhance human interpretation for efficient detection and characterization with the utilization of AI approaches.

The purpose of the present work is to develop a generic approach for the automatic identification of the various structural layer lying within GPR B-Scan radargrams. The novelty of this study is substantiated through the amalgamation of three components: first, the methodology followed to acquire the data, create the ground truth dataset and pre/post-process of the data, second the classifier utilized for developing the predictive model and third the use case itself as it enabled the creation of a high-quality ground truth dataset. Compared to other approaches found in literature study, the present one manages a sufficient model performance for 3 out of the 5 classes with using a very small dataset for model training and validation, suggesting that the approach followed is at least promising and the model performance could dramatically get improved with the inclusion of some more data.

2. USE CASE: THE HOLY AEDICULE OF THE HOLY SEPULCHRE

A unique monument located in Jerusalem (the south side before the rehabilitation works is presented in Figure 1) being the most important site of Christianity, as it is the place where Jesus Christ was buried and resurrected is the Holy Aedicule of the Holy Sepulchre (Lavas, 2009). It is actually a complex structure, embedding remnants of the original structure (Holy Rock) and the Tomb of Christ, as well as the many construction phases, of its rich history of almost two millennia, throughout which it was destroyed, reconstructed restored and rehabilitated many times (Biddle 1999; Mitropoulos, 2009; Moropoulou et al., 2013). Some years after the latest restoration works took place to amend the destruction caused by a catastrophic fire in the Church of Resur-

rection in 1808, the Holy Aedicule of the Holy Sepulchre confronted with deformation issues upon its facades. The Holy Aedicule rehabilitation that was completed in March 2017 by NTUA aimed to address the deformation problems encountered, according to the findings and proposals of NTUA's diagnostic study (Moropoulou et al., 2016). The phases of the rehabilitation works, follow a strict timeline starting from the dismantling of the facades building stones, the cleaning of the disintegrated mortars, the repointing of the joints, and the grouting and reinforcement of the structure, to the cleaning, protection and repositioning of the building stone (Alexakis et al., 2018). The GPR B-Scan radargrams acquired during the diagnostic study were analyzed and the results were validated through the respective rehabilitation phases resulting in a high-quality ground truth dataset utilized in the present study.

Figure 1. The south side of the Holy Aedicule prior to the rehabilitation works (photo courtesy of A. Moropoulou)

3. GROUND PENETRATION RADAR IMAGE GENERATION

3.1. The GPR technique

Ground penetrating radar (GPR) is a non-destructive geophysical technique which is based on the propagation and spatial/temporal analysis of electromagnetic radiation transmitted through the prospected structure. A typical GPR con-sists of two antennae (one emitting and one receiving, often included in the same casing), a main unit that controls the electromagnetic pulse and a display unit. Short electromagnetic waves (pulses) are emitted from the GPR antenna located on the surface of a structure and are transmitted through low-loss dielectric mate-rials within the prospected volume. As presented in **Figure 2** The receiving GPR antenna (co-located with the

emitting antenna) detects the reflected electromagnetic wave from within the prospected volume which corresponds to primary reflections, multiple echoes from secondary reflections or wave interference phenomena (Daniels (Ed.), 2004).

GPR can detect variations in the dielectric properties of the materials which can be used to identify subsurface features, structures and layers or different humidity levels within the structures or soil investigated. The GPR surveys are typically conducted either in 2-D or 3-D approaches. The most common approach and the one utilized in this study, is the 2-D approach where the GPR antenna (typically combines emitting and receiving dipoles) moves along a profile, whereas the spatial position of the antenna is recorded. At, regular intervals, at each point along the path, the GPR transmitter antenna emits a short electromagnetic pulse. The co-located receiving antenna

records the intensity of the receiving pulse for the duration of a pre-set time window (in the order of nanoseconds). As a result, at each point a point-trace is received which records the intensity of the received pulse vs the two-way time. As the antenna casing moves along the path, the procedure is repeated, and corresponding point traces are received.

For ease of display, the point traces are not presented as "wiggle" traces (i.e., much like a oscillograph). Instead, each wiggle trace is converted by the GPR software into a pixelized line, where the color or the gray-scale intensity of each pixel corresponds to the intensity (positive or negative) of the received pulse whereas the pixel's location along this line corresponds to the two-way time that the pulse was received. By placing each of these pixelized lines next to each other, an "image" of the prospected section is received. The horizontal axis of this image corresponds to the position of the GPR antenna, whereas the vertical axis of the image corresponds to the two-way time

for the pulse. The color or gray-scale intensity of each pixel of this image corresponds to the intensity of the received signal. The location of each pixel defines the position of the antenna over the surface (x-axis) and the two-way time that the intensity of the pixel corresponds to. Note that since the vertical axis of such an image is not scaled in distance unit, but in units of time, it is not readily convertible to distance units. The reason is that the electromagnetic pulse propagates with different velocities depending on the electromagnetic properties of the materials. Thus, if the layering of the prospected structure is not known in detail, exact pulse velocities per layer cannot be easily attributed, and thus the conversion of the vertical axis from time-units into distance-units is not easily performed. Often, however, an average pulse velocity is assigned, to aid in the conversion of the vertical axis into depth.
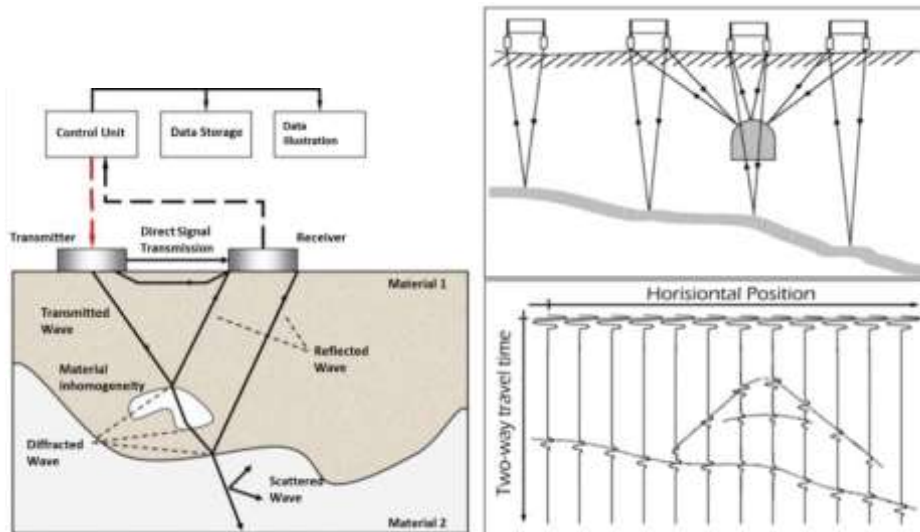

Figure 2. Left: Principle of operation and configuration of GPR. Right: Schematic overlay of 1-D point traces, as the GPR antenna moves along the horizontal path over the prospected surface, to create a 2-D section of the soil (schematic courtesy of K. Lampropoulos).

After the application of various signal filters (e.g. time-zero adjustment, background removal, gain enhancement, band pass filtering, predictive deconvolution) a radargram is created in the form of a 2-dimensional tomographic section of the prospected area like the one presented in Figure 3. This data post-processing is due to the low resolution (decreased sensitivity in centimeter-sized targets) GPR signals and the frequency of the GPR transmitted electromagnetic waves (the higher the pulse frequency the more intense the wave amplitude attenuation). Thus, signal processing improves the interpretation of the GPR raw data by increasing temporal resolution (with the

use of deconvolution and denoising filters) (Daniels (Ed.), 2004). On the one hand, signal processing is a prerequisite manual step to filter clutter and noise out of useful information and cannot be automated as different use cases might bring different needs (i.e., increased resolution instead of high penetration depth). On the other hand, pattern recognition automation could enhance human interpretation for efficient detection and characterization with the utilization of AI approaches. This is more evidently presented in the following section where after the signal processing step, the various structural layers are recognized and denoted before feeding in the classification model.
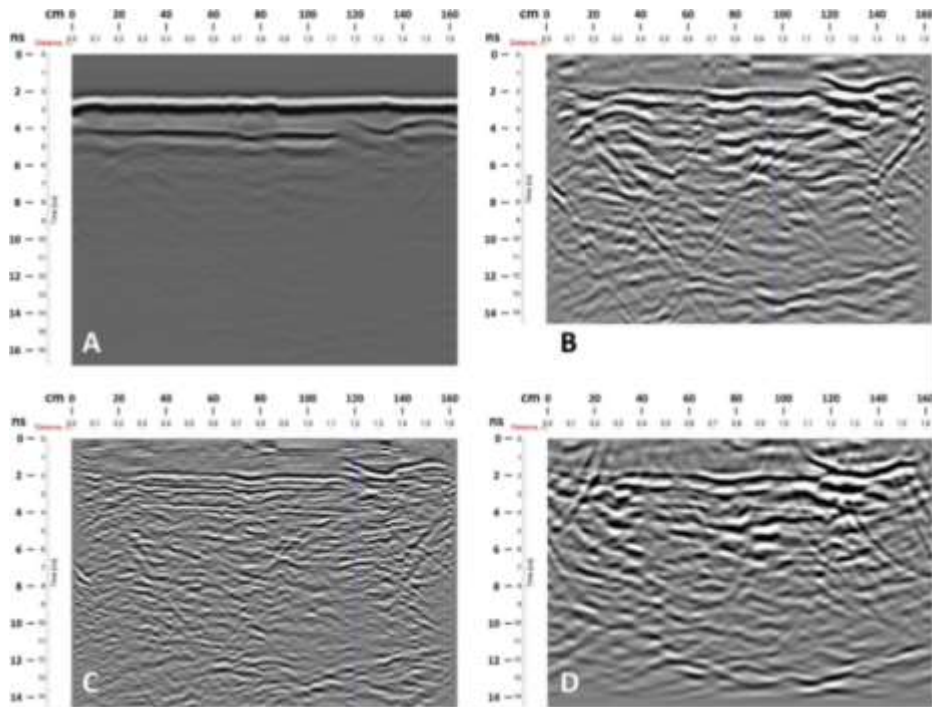
Figure 3. A) Typical non-processed radargram over the Marble relief of Christ resurrection within the burial chamber of the Holy Aedicule; B) After application of the data processing filters; C) Application of predictive deconvolution to radargram; D) Application of the Stolt F-K Migration routine to radargram (Lampropoulos et al., 2017).

3.2. Structural layers identification in GPR analysis – Input data for Deep Learning

A typical radargram over the façade panel S4 of the Holy Aedicule with a horizontal west-east orientation at a height level of 120cm is presented in Figure 4. The blue-colored wiggle trace indicates the temporal variation of the received pulse when the GPR antenna was over a position 10cm from the starting point. The higher intensity values of the pulse signal at certain depths corresponds to the presence of interfaces within the masonry (or alternatively of very different electrical properties of the materials) which result in significant reflections originating from these locations.

The GPR user studies each radargram (scan) and based on their experience as well as available documentation (plans, descriptions etc.) tries to identify and mark each target observed within. Those 2-D scans are then "connected" in a 3-D software to describe identified features (e.g. underground pipes, or masonry layers). In cases where extensive and well overlapping 2-D scans are not feasible, the 3-D imaging of the prospected structure is not a trivial task. The use case of the Holy Aedicule (Lampropoulos et al., 2017) is exactly that, as its structure has exterior surfaces that did not allow the conduction of extensive long parallel and/or transverse GPR scans. Instead, due to the morphology of the exterior surfaces, GPR prospection was limited to small, isolated areas of each façade, allowing the implementation of small-length horizontal or vertical scans. Moreover, there was no prior information regarding the internal layering of this structure, especially regarding the potential presence of remnants of the original rock.
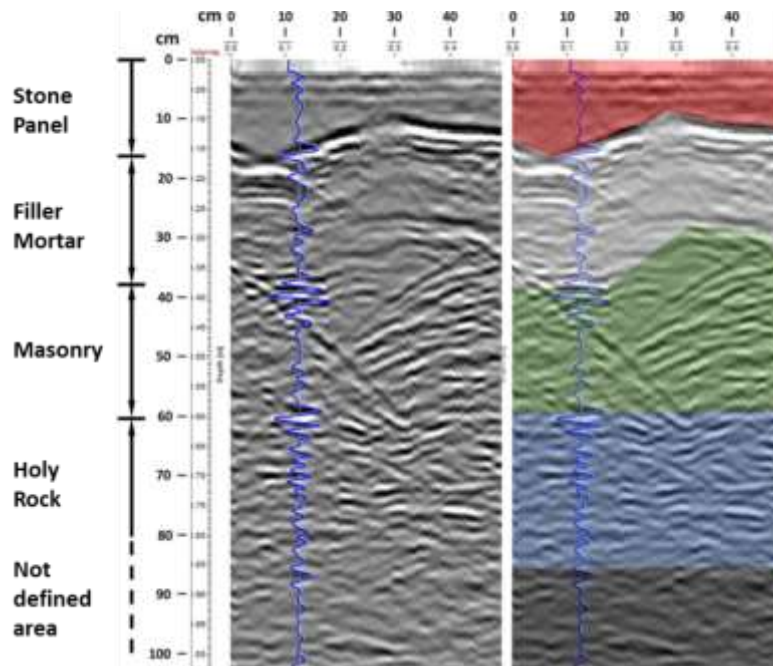
Figure 4. Radargram at façade panel S4, with a horizontal west-east orientation, at a height level of 120 cm, after processing and depth conversion. A single wiggle trace is displayed above the radargram which facilitates the discrimination of the various surface layers.

A series of 19 selected distance vs. time GPR scans, coming from two façade panels (N3 and N4, as presented in Fig.5, were processed (signal filters) and target identification was performed for each scan aiming to annotate the main masonry layers, i.e. the exterior stone panel, the filler mortar, the masonry, the Holy Rock and an unidentified area, as presented with colors in Fig.4. This is a typical image segmentation problem and the approach and methodology followed to resolve it is described in the coming session.

Figure 5. The North side of the Holy Aedicule before the rehabilitation works. In the white frames the two panels where the GPR measurements took place (photo courtesy of A. Moropoulou)

4. METHODOLOGY

4.1. Data pre-processing

As described in the previous section, the eventual dataset utilized for the needs of this study consists of 19 images illustrating the Holy Aedicule of the Holy Sepulchre masonry multilayer patterns examined during the diagnostic survey campaign, took place prior to the rehabilitation. Those layers have been revealed during the rehabilitation works and the certain scans measurement (ground truth images) have been validated on hands. The ground truth images contain at most 5 different areas, corresponding to the various material layers: 1) external stone panel, 2) filler mortar, 3) masonry, 4) Holy Rock and 5) an area where the interpretation of GPR radargrams is not considered reliable due to the increased depth and pulse attenuation. This is described as a typical computer vision image segmentation problem where there are 5 different colors/masks each of those depict a different ground pattern found in the original image; red for stone panel, white for filler mortar, green for masonry, blue for Holy Rock and black for the area where GPR measurements are not considered reliable due to wave attenuation. A pair of source - ground truth images is presented in Fig.6.
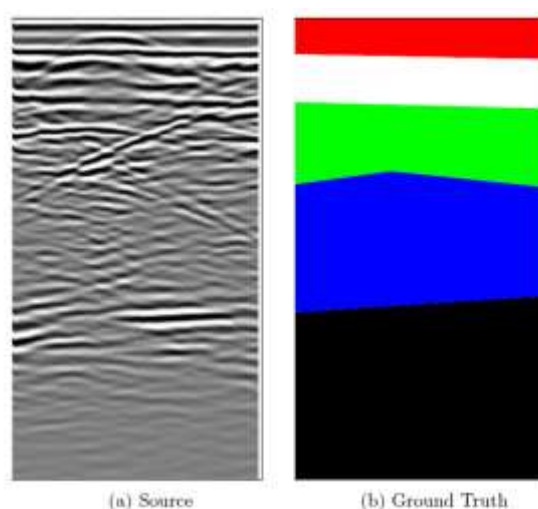

(a) Source   (b) Ground Truth

Figure 6. The left figure shows the original image of the ground pattern, while the right one depicts the ground truth labels. The red, white, green, blue and black colours depict the stone panel (surface), filler mortar, masonry, Holy Rock and unidentified area structural layers, respectively.

The first section of the data processing is described in **Figure 7** and is related to the preparation of the data used for the training/validation of the model. The initial size of both the source and the ground truth images is approximately 339x528 pixels. Since the number of the source images was small, it was necessary to break the images into several patches in order to train the model appropriately. Below, the pre-processing stages are presented shortly:

In this stage, both the source and the ground truth images were cropped perimetrically to ensure the absence of potential border abnormalities and to achieve a common shape among the images. The new shape of the image is approximately 310x510.

In this step, the images were split in a certain number of patches. The exact size of the patches along with the distribution of the patches in the image area was determined using trial and error techniques.

At this point, a multichannel image/array was created for each ground truth image. Each channel of the new array corresponds to a single label of the initial ground truth image. Thus, the multichannel image/array has the following shape: patch Width x patch Height x 5.
Finally, the train, validation and test sub-datasets are produced by using 70%, 20% and 10% of the initial number of patches respectively.

The training and validation datasets are used to train and validate the model, described in the coming section, whereas test dataset is utilized for the assessment of the model.
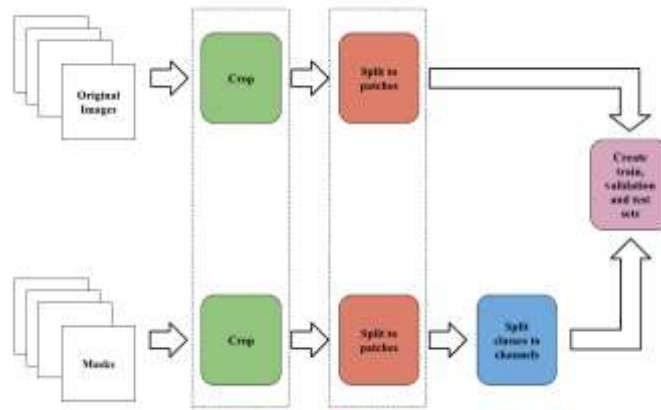
Figure 7. Data pre-processing workflow followed to conclude in the train, validation and test datasets for training validating and evaluating the model performance

4.2. Convolutional Neural Network U-Net Architecture

The core of our approach is the deep convolutional network of U-Net, successfully applied for segmentation and classification of medical image data (Ronneberger et al., 2015) which in fact is the structure of the model applied for data classification in the present study. The novelty in the present approach is summarized in the successful application of a model initially developed for another type of data, on a very small of appropriate pre-processed data coming from a historic monument. The reason why U-Net has chosen is that the model implements convolutional kernels for global-local data processing and therefore, increasing classification performance with just a few training images.

The main concept behind these networks, compared to common convolutional neural networks, is to supply the latter by successive layers, utilizing up-sampling operators resulting in the increase of the output resolution, making the successive layer to learn to assemble a precise output. The large number of feature channels within up-sampling operators allow the network to propagate context information to higher resolution layers. In this way, the contracting path is less or more symmetric to the expansive part, giving a U-shaped architecture. To make a pixel prediction in the border region of the image, the input image is mirrored, and the missing context is extrapolated. The utilized UNet model architecture is illustrated in **Figure 8** summarizing its major features in:

- Blue arrows depict the combination of convolution and ReLU operations.
- Red arrows represent the Max-Pooling operations, resulting in the decreasing of the patch size.
- Yellow arrows symbolize the up-sampling operations.

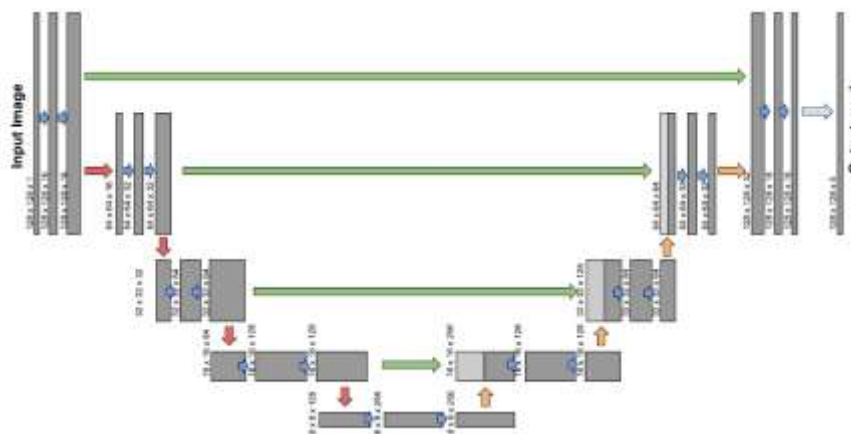Copy and concatenation procedures take place across the green arrows.

Figure 8. U-Net model Architecture (Ronneberger et al., 2015)

After the training of the model on the corresponding training data of the dataset, the U-Net model is assessed on the test dataset. The procedure of evaluation is summarized in the following steps:

- The model generates the multichannel prediction of the current image patch. Each channel represents the corresponding color of the different ground truth layers.
- The multichannel patch is being converted to a single RGB patch.
- The predicted image is being reconstructed by the corresponding predicted patches.
- The original ground truth image is being reconstructed by the corresponding ground truth patches.

- Both the original and the predicted reconstructed images are combined to generate the evaluation metrics.

The learning curve, generated during the training process, is presented in **Figure 9**. On the one hand, the validation loss stops improving after the 3rd epoch and begins to decrease afterward making a kind of oscillation. On the other hand, the training metric continues to improve as the model seeks to find the best fit for the training data. Thus, the best model fit is achieved when the validation error is at its' lowest level (3rd epoch), after which overfitting takes over, suggesting the need for training the model with more data.
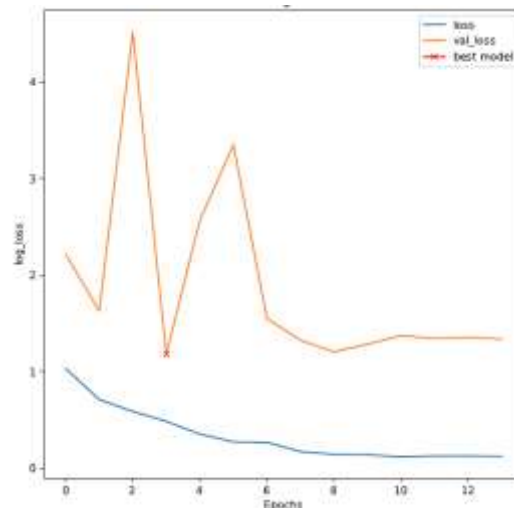
Figure 9. Model learning curve where best fit is achieved at the 3rd training epoch

4.3. Model Assessment

The model assessment pipeline is presented in **Fig. 10**, where after the model is trained and validated over the train and validation sets, respectively, the test dataset is used to generate the model predictions. Model predictions then are compared with the original test dataset in pixel level and the model performance is evaluated upon the accuracy, precision, recall and f1 score metrics for each one of the 5 different classes.
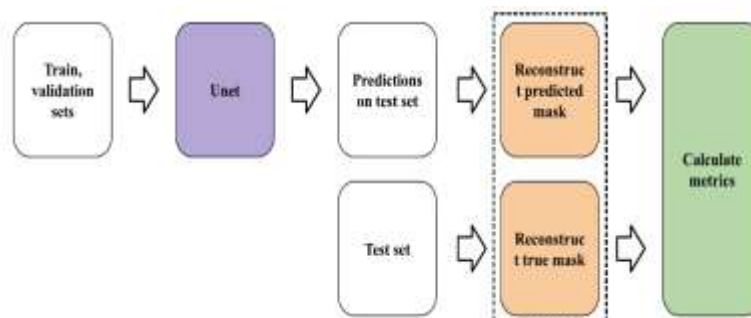
Fig. 10. Model assessment pipeline

The evaluation results for every class are illustrated in **Figure 11**. Classes 0, 1, 2, 3, 4 correspond to the colors black, red, green, white, blue and subsequently to the respective structural layer of the original ground truth image, presented accordingly in **Table 1**. The model achieves great performance for classes 0 and 1 (black, red) especially with regards to the accuracy and precision metrics whereas performance for classes 2 and 3 (green, white) is more mediocre. In particular, the accuracy for class 2 is almost 99% suggesting that the model has correctly predicted observation over the total observations for this class but as this class lacks symmetry with respect to the other classes (this area correspond to the stone

panel which is smaller compared to the others) the other metrics has to be accounted for the assessment. The ratio of correctly predicted positive observations to the total predicted positive observations (precision) is almost 80% while recall (the ratio of correctly predicted positive observations to all observations in the actual class) and f1 score (the weighted average of precision and recall.) is above 80% suggesting a very high model performance for the specific class. More mediocre model performance is achieved for classes 2 and 3 while model seem to underperform for class 4 having approximately 60% accuracy and less than 50% for all the other metrics.
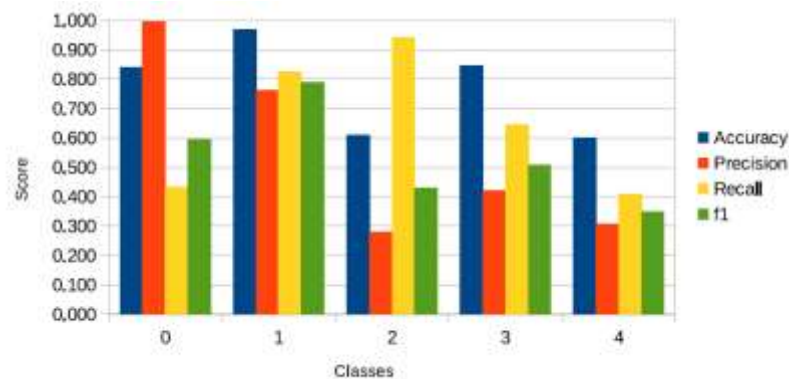

Figure 11. Test set evaluation metrics. Classes 0, 1, 2, 3, 4 correspond to the colors black, red, green, white, blue of the original ground truth image accordingly

Table 1. Allocation of classes, colors and the RGB values with the respective structural layers

Class ID	Color	RGB Value	Structural Layer
0	Black	(0, 0, 0)	Unidentified area
1	Red	(255, 0, 0)	Stone panel
2	Green	(0, 255, 0)	Masonry
3	White	(255, 255, 255)	Filler mortar
4	Blue	(0, 0, 255)	Holy Rock

5. DISCUSSION AND CONCLUSION

The main purpose of the present work is the development of a tool for enhancing, supporting and subsequently manage automatic structural pattern recognition within GPR B-Scan radargrams. Thus, the outcome of the applied methodology shall be evaluated as a supporting "tool" for the GPR user to aid them in pattern recognition. GPR is a geophysical method, and as such relies heavily on the materials di-electric

properties of the prospected area and structure under examination. The identified features/patterns are in effect differentiation of materials' electrical properties, and not necessarily true interfaces. Moreover, like most NDTs applied on CH assets benefit from prior knowledge of some basic information regarding their structural layers; However, in CH applications this is more than often the exception rather than the norm. Nonetheless, the current work emphasizes the

potential for pattern recognition in GPR as a supporting tool for GPR analysis.

The use case selected (Holy Aedicule) in fact demonstrates the feasibility of the developed methodology, despite the limited performance of the classifier for certain classes. It should be emphasized that the pre-processing of the GPR raw data is still necessary since filtering of the raw data actually "brings-out" useful information hitherto "hidden" within the instrument "noise". Specialized GPR software is used for this, therefore the raw data cannot, yet, be used directly for this methodology.

Moreover, at this stage of development, the GPR scans used are distance vs. time scans and not the more user-friendly distance vs. depth scans. The reason is that the conversion of timescale into depth-scale, requires the definition of appropriate velocity models in the GPR software used. These velocity models, nonetheless, require knowledge of the actual layering of the structure examined as well as the values for the pulse velocity per layer, so that the time-depth transformation can proceed. This, arguably, seems to contradict the main scope of this attempt, in the sense that if the user already knows the layering of the structure, then they do not potentially need this methodology, but this does not actually have an impact on the ability of the model to learn from the radargrams as the aim to manage to discriminate the classes from another (structural layers) no matter what their size. However, this regards the second level (future work) of analysis, where deep learning will identify layers in time-scaled GPR radargrams, suggest appropriate velocity models, with which the

GPR software can convert the radargrams in depth-scaled tomographies. The user may then either fine tune the velocity models, or alternatively use these results to identify the required features in the examined structure and assess its layering or state of preservation.

Another aspect that needs consideration is the limited number of images used to train the model as 19 images in a computer vision image segmentation classifier with 5 classes are considered few. This, in turn, highlights the importance of the validation and test datasets and especially the way they are determined for the model evaluation as an inappropriate choice of validation (3 images) and test (1 image) datasets could lead to radical different model performance. Despite the fact that the cross-validation approach followed did not raise any concern regarding the model predictive performance, the need of including more data for model training is imperative and it will be served in future work supplementing this study. As there are enough data coming from the rest of external stone panels that first need to be manually pre-processed after examining the possibility of using the distance vs. depth GPR scans, as described in the previous paragraph.

To summarize, despite the limitations and drawbacks, the models' classification performance is quite promising as it manages remarkable classification accuracy and precision for at least 3 (out of 5) classes utilizing a very small dataset. Accounting and resolving some or all of the limitations will certainly lead to drastic model performance improvement.

AUTHOR CONTRIBUTION

ACKNOWLEDGEMENTS

REFERENCES

Alexakis, Emm., Delegou, E.T., Lampropoulos, K.C., Apostolopoulou, M., Ntoutsi, I., Moropoulou, A. (2018). NDT as a monitoring tool of the works progress and the assessment of materials and rehabilitation interventions at the Holy Aedicule of the Holy Sepulchre. *Construction and Building Materials, 189*, pp. 512–526.

Aydıngün, Ş., Kurban, Y.C., Yalçıner, C.Ç., Büyüksaraç, A., Gündoğdu, E., Altunel, E. (2020). High-resolution ground penetrating radar investigation of yerebatan (basilica) cistern in istanbul (Constantinople) for restoration purposes. *Mediterranean Archaeology and Archaeometry* Vol. 20, No 3, pp. 13-26 DOI: 10.5281/zenodo.3930402.

Anzani, A., Binda, L., Lualdi, M., Tedeschi, C., Zanzi, L. (2006). Use of Sonic and GPR Tests to Control the Effectiveness of Grout Injections of Stone Masonry. *ECNDT, 3*, pp. 1-7.

Biddle, M. (1999). *The Tomb of Christ.* Sutton: Gloucestershire England.

Cartz, L. (1995). *Nondestructive Testing: Radiography, Ultrasonics, Liquid Penetrant, Magnetic Particle, Eddy Current.* ASM International. doi:ISBN: 978-0-87170-517-4.

Daniels J. D. (Ed.). (2004). *Ground Penetrating Radar - 2nd Edition.* London: The Institution of Electrical Engineers, London, United Kingdom. doi:ISBN 0 86341 360 9.

Fiorucci, M; Khoroshiltseva, M; Pontil, M; Traviglia, A; Del Bue, A; James, S;. (2020). Machine Learning for Cultural Heritage: A Survey. *Pattern Recognition Letters, 133*, 102-108. doi:https://doi.org/10.1016/j.patrec.2020.02.017.

Garrido, I., Erazo-Aux, J., Lagüela, S., Sfarra, S., Ibarra-Castanedo, C., Pivarčiová, E., Gargiulo, G., Maldague, X., Arias, P. (2021). Introduction of Deep Learning in Thermographic Monitoring of Cultural Heritage and Improvement by Automatic Thermogram Pre-Processing Algorithms. *Sensors, 21* (750). doi:https://doi.org/10.3390/s21030750.

Jaén-Candón, M., Jiménez-Hernández, A., Carrasco- Gómez, I., Peña-Ruano, J., Teixidó-Ullod, T. (2019). The intramural chariot racing stone barrier at Carteia (Spain): geophysical survey and verification by archaeological test excavation *Mediterranean Archaeology and Archaeometry* Vol. 19, No 3, pp. 139-156, DOI: 10.5281/zenodo.3583065

Küçükdemirci, M., Sarris, A. (2020) Deep learning based automated analysis of archaeo-geophysical images. *Archaeol. Prospect.* 2020, 27, pp. 107–118 https://doi.org/10.1002/arp.1763.

Lampropoulos, K.C., Moropoulou, A., Korres, M. (2017). Ground penetrating radar prospection of the construction phases of the Holy Aedicula of the Church of the Holy Sepulchre, in correlation with architectural analysis. *Construction and Building Materials, 155*, pp. 307-322.

Lavas, G. (2009). The Holy Church of the Resurrection in Jerusalem. Publisher: The Academy of Athens, 194 p., ISBN-13: 9789604041398 (in Greek).

Leckebusch, J., Weibel, A., Bühler, F. (2008). Semi-automatic feature extraction from GPR data for archaeology. *Near Surf. Geophys.* 2008, 6, pp. 75–84.

Levy, T. E., Sideris, T., Howland, M., Liss, B., Tsokas, G., Stambolidis, A., Fikos, E., Vargemezis, G., Tsourlos, P., Georgopoulos, A., Papatheodorou, G., Garaga, M., Christodoulou, D., Norris, R., Rivera-Collazo, I., and Liritzis I. (2018) At-Risk World Heritage, Cyber, and Marine Archaeology: The Kastrouli–Antikyra Bay Land and Sea Project, Phokis, Greece , Springer International Publishing AG In T.E. Levy, I.W.N. Jones (eds.), *Cyber-Archaeology and Grand Narratives, One World Archaeology*, pp. 143-230. http://dx.doi.org/10.1007/978-3-319-65693-9_9.

Manataki, M., Vafidis, A., Sarris, A. (2021). GPR Data Interpretation Approaches in Archaeological Prospection. *Appl. Sci.*, 11, 7531. https://doi.org/10.3390/app11167531

Martini, R., Carvalho, J., Barraca, N. , Arêde, A., Varum, H. (2017). Advances on the use of non-destructive techniques for mechanical characterization of stone masonry: GPR and sonic tests. *Procedia Structural Integrity, 5*, pp. 1108-1115.

Mitropoulos, Th. (2009). The Church of Holy Sepulchre – *The Work of Kalfas Komnenos 1808-1810,* Publisher: European Centre of Byzantine and Post-Byzantine Monuments, 304 p., ISBN-13: 9789608842373 (in Greek).

Moropoulou, A., Korres, E., Georgopoulos, A., Spyrakos, C. (2016). Integrated diagnostic research project and strategic planning for materials, interventions conservation and rehabilitation of the Holy Edicule of the Holy Sepulchre in the Holy Church of the Resurrection in Jerusalem, 109 p., ISBN 978-618-82612-0-4

Moropoulou, A., Avdelidis, N. P., Karoglou, M., Delegou, E. T., Alexakis, Emm., Keramidas, V. . (2018). Multispectral Applications of Infrared Thermography in the Diagnosis and Protection of Built Cultural Heritage. *Applied Sciences, 8*(2), 26. doi:https://doi.org/10.3390/app8020284

Moropoulou, A., Labropoulos, K. C., Delegou, E. T., Karoglou, M., Bakolas, A. . (2013). Non-Destructive Techniques as a tool for the protection of Built Cultural Heritage. *Constr. Build. Mat., 48*, pp. 1222-1239.

Ronneberger, O., Fischer, P., Brox, T. (2015). U-Net: Convolutional Networks for Biomedical Image Segmentation. *Medical Image Computing and Computer-Assisted Intervention (MICCAI), 9351*, pp. 234--241. Retrieved from https://arxiv.org/abs/1505.04597v1.

Savvaidis, A., Tsokas, G., Liritzis, I., Apostolou, M. (1999). The location and mapping of ancient ruins on the castle of Lefkas (Greece) by resistivity and GPR methods. *Archaeological Prospection*, 6, pp. 63-73.

Travassos, X., Avila, S., Ida, N. (2020). Artificial Neural Networks and Machine Learning techniques applied toGround Penetrating Radar: A review. *Applied Computing and Informatics, 17*(2), 296-308. doi:https://doi.org/10.1016/j.aci.2018.10.001.

Vidovszky, I. (2016). Impact-based Diagnostic Approach for Maintenance Monitoring of Historic Buildings. *Procedia Engineering, 164*, pp. 575-582.

Yue, Y., Liu, H., Meng, X., Li, Y., Du, Y. (2021). Generation of High-Precision Ground Penetrating Radar Images Using Improved Least Square Generative Adversarial Networks. *Remote Sens.* 2021, 13, 4590. https://doi.org/10.3390/rs13224590.